Title
Self-Catalyzed Rechargeable Lithium-Air Battery by in situ Metal Ion Doping of Discharge Products: A Combined Theoretical and Experimental Study

Journal
Energy & Environmental Materials, 6(1)

ISSN
2575-0348

Authors
Yuan, Mengwei
Sun, Zemin
Yang, Han
et al.

Publication Date
2023

DOI
10.1002/eem2.12258

Article category: Full Paper
Subcategory: Lithium Air Battery

Self-Catalyzed Rechargeable Lithium-Air Battery by in-situ Metal Ion Doping of Discharge Products: A Combined Theoretical and Experimental Study

Mengwei Yuan,[a,b,#] Zemin Sun,[a,#] Han Yang,[a] Di Wang,[a] Qiming Liu,[c] Caiyun Nan,[a] Huifeng Li,[a] Genban Sun,[a,] and Shaowei Chen[c,*]*

Dr. M. W. Yuan, Dr. Z. M. Sun, H. Yang, D. Wang, Dr. C. Y. Nan, Dr. H. F. Li, Prof. G. B. Sun
Beijing Key Laboratory of Energy Conversion and Storage Materials Institution, College of Chemistry, Beijing Normal University, Beijing 100875 (P. R. China)
E-mail: gbsun@bnu.edu.cn

Dr. M. W. Yuan
Department of Physics and Applied Optics Beijing Area Major Laboratory, Beijing Normal University, Beijing 100875 (P. R. China)

Mr. Q. M. Liu, Prof. S. W. Chen
Department of Chemistry and Biochemistry, University of California, 1156 High Street, Santa Cruz, California 95064, United States
E-mail: shaowei@ucsc.edu

Keywords: self-catalysis; lithium-air battery; Co^{2+}-doped Li_2O_2; in situ electrochemical doping; density functional theory

Abstract

Lithium-air battery (LAB) has emerged as a viable electrochemical energy technology; yet a substantial overpotential is typically observed, due to the insulating nature of the discharge

product Li_2O_2 that hinders the reaction kinetics and device performance. Furthermore, finite solid-solid/-liquid interfaces are formed between Li_2O_2 and catalysts and limit the activity of the electrocatalysts in battery reactions, leading to inadequate electrolytic efficiency. Herein, in-situ doping of Li_2O_2 by select metal ions is found to significantly enhance the LAB performance, and Co^{2+} stands out as the most effective dopant among the series. This is ascribed to the unique catalytic activity of the resulting Co-O_x sites towards oxygen electrocatalysis, rendering the LAB self-catalytically active. Theoretical studies based on density functional theory calculations show that structural compression occurs upon Co^{2+} doping, which lowers the energy barrier of Li_2O_2 decomposition. Results from this study highlight the significance of in situ electrochemical doping of the discharge product in enhancing the performance of LAB.

1. Introduction

With the development of (hybrid) electrical vehicles, the demand for effective energy conversion and storage technologies has never been higher,[1-4] as conventional lithium-ion battery is approaching its theoretical limit (500 Wh kg^{-1}) for the emerging energy market.[5, 6] Lithium-air battery (LAB) represents a promising alternative, exhibiting a remarkable theoretical energy density of 11,400 Wh kg^{-1}.[7] Yet it suffers from a low round-trip efficiency and poor cyclability, mainly due to the sluggish reaction kinetics.[8, 9] In particular, the intrinsically low electrical and ionic conductivity of the discharge product Li_2O_2 is found to hamper the kinetics of oxygen reduction/evolution reactions (ORR/OER) during the discharge/charge processes.

To mitigate these issues, extensive studies have been carried out focusing on the design and engineering of bifunctional electrocatalysts and redox mediators to facilitate the ORR and OER electrocatalysis, reduce the overpotential, and enhance the battery life. These entails electrocatalysts based on noble metals (e.g., PtAu,[10] Ru,[11, 12] Pd,[13, 14] and Ir[15]) and transition metals (e.g., MnO_2,[16, 17] Co_3O_4,[18, 19] CoO,[20] Co_4N,[21] MoS_2,[22, 23] Co_2O_4,[24] Mo_2C,[25] and metal-organic frameworks[26, 27]), as well as redox mediators (e.g., LiI,[28] tetrathiafulvalene,[29, 30] TEMPO,[31] 2,5-di-tert-butyl-1,4-benzoquinone (DBBQ),[32] and $V(acac)_3$[33]). Of these, redox mediators can act as liquid electrocatalysts and facilitate the ORR and/or OER process by three mechanisms, redox-shuttle, complex intermediate, and product transformation.[34] In addition, the formation of nano-sized, defective, and amorphous Li_2O_2 as the discharge product that exhibits enhanced charge transport and electro-oxidation kinetics can also efficiently reduce the overpotential and improve the energy conversion efficiency.[35-39] Similar progress has been

achieved by deliberate control of the nucleation and growth of the discharge product from Li_2O_2 to LiO_2.[40, 41] Nevertheless, the formation of both solid-solid and solid-liquid interfaces between the discharge product and electrocatalysts has been found to limit the electron-transfer kinetics of the ORR and OER processes, leading to inadequate electrocatalytic performance. These results suggest that it is critical to develop effective oxygen electrocatalysts free of multiphase interfaces, where self-catalysis represents a unique strategy to enhance the device performance. Towards this end, chemical doping of the electrode materials represents an effective route, due to ready manipulation of the materials density of states, band structures, and electrical conductivity,[42-45] leading to enhanced electrochemical activity, stability, and ultimately device performance. [46-49] For instance, Lyu et al. and Dai et al. recently showed that doping of Na^+ and K^+ into the Li_2O_2 matrix led to marked improvement of the energy efficiency of LAB.[38, 50] Meanwhile, high-throughput screening and machine learning methods have been playing an important role in advancing LAB research.[51, 52]

In the present study, we carry out theoretical studies based on density functional theory (DFT) calculations and observe that doping of the discharge product Li_2O_2 by select metal ions can markedly enhance the LAB performance. Experimentally, Li_2O_2 is in situ doped with a series of metal ions in the discharge process, and cobalt stands out as the most effective dopant among the series. Specifically, $CoLi_{2-x}O_2$ is found to exhibit markedly enhanced electrical conductivity, elongated O-O bond, and reduced energy barrier for Li_2O_2 decomposition, as compared to pristine Li_2O_2. Also, in the recharge process, the Co-O_x sites act as the active centers to facilitate the decomposition of $Li_{2-x}O_2$, minimize the formation of multiphase interface, and realize product self-catalysis, in good agreement with results from DFT calculations. Remarkably, the overpotential of such self-catalyzed LAB (SCLAB) is reduced to only 0.84 V, and the cycling stability is also significantly enhanced with a low polarization, as compared to traditional LAB (TLAB).

2. Results and Discussion

As mentioned earlier, Li_2O_2 is an insulating discharge product in TLAB, which hampers the reaction kinetics and limits the device performance. Such an issue can be effectively mitigated by ion doping into the discharge product. In the present study, this was first examined by theoretical studies based on DFT calculations (details in the Supporting Information) (**Figure 1**). Upon Co^{2+} doping into the $Li_{2-x}O_2$ matrix ($CoLi_{62}O_{64}$, self-consistent model obtained by continuously adjusting the theoretical model and the amount of additives in experiments) (Figure 1a), DFT

calculations show that the Li-O bonds around the Co-O_x center were distorted with the bond length shortened to 2.14 Å (site 1) and 1.96 Å (site 2), in comparison to 2.16 Å of pristine Li_2O_2 (Figure 1c). Concurrently, the O-O bond length at site 1 was increased to 1.669 Å from 1.542 Å in Li_2O_2; and the Li-O-Li angle was enlarged to 103.0º (site 1) and 96.4º (site 2) from 79.4º in Li_2O_2. These changes indicate apparent structural compression due to the introduction of high-electronegativity cobalt, resulting in electron enrichment in the direction of the active center, which could be observed in the 2D charge distributions for Co^{2+}-doped $Li_{62}O_{64}$ and $Li_{64}O_{64}$ (Figure 1d), leading to a lower energy barrier for $CoLi_{62}O_{64}$ decomposition in the electrochemical ORR/OER processes, in comparison to pristine Li_2O_2.

Similar results were obtained when other metal ions (e.g., Na^+, K^+, Mg^{2+}, Al^{3+}, Ca^{2+}, Mn^{2+}, Fe^{2+}, Co^{2+}, Ni^{2+}, Cu^{2+}, and Zn^{2+}), either electrochemically active or inactive, were doped into the $Li_{2-x}O_2$ matrix (Figure 1e and S1-S3, Table S1). For instance, with Al^{3+} doped into $Li_{2-x}O_2$ ($AlLi_{61}O_{64}$, Figure 1b), the bond lengths of Li-O and O-O at the corresponding site 1 were changed to 2.21 Å and 1.546 Å, respectively. These results indicate that incorporation of either electrochemically inactive or active dopants into $Li_{2-x}O_2$ can effectively manipulate the micro-structure and property of the discharge product. Among the series, cobalt was found to exert the most significant impacts. Figure 1f-1h show the corresponding total density of states (TDOS) of three representative structures, Co^{2+}-doped $Li_{2-x}O_2$ ($CoLi_{62}O_{64}$, Figure 1a), Al^{3+}-doped $Li_{2-x}O_2$ ($AlLi_{61}O_{64}$, Figure 1b) and pristine Li_2O_2 ($Li_{64}O_{64}$, Figure 1c), where one can see that the band gap decreases in the order of $Li_{64}O_{64}$ > $AlLi_{61}O_{64}$ > $CoLi_{62}O_{64}$. The markedly enhanced electrical conductivity of $CoLi_{62}O_{64}$ indeed played an important role in improving the LAB performance (vide infra). [53, 54] In addition, the TDOS of $CoLi_{62}O_{64}$ was located mostly near the Fermi level, suggestive of a high activity in electron-transfer reactions,[55] in contrast to pristine Li_2O_2.[56]

In battery reactions, the growth of Li_2O_2 is also important. Thus, slab models were also constructed to investigate the adsorption of Li_2O_2 molecules onto the generated products, so as to highlight the difference between the doped and undoped Li_2O_2. Both Al-Li_2O_2 and Co-Li_2O_2 can be seen to display a superior adsorption capability (Figure S4), as compared to undoped Li_2O_2, suggesting an enhanced driving force for the growth of Li_2O_2. Notably, even after the adsorption of Li_2O_2 molecules, Co-Li_2O_2 retained high conductivity due to the optimization of the oxygen p electrons by Co^{2+} doping (Figure S5). That is, Co^{2+} doping facilitated not only the growth of Li_2O_2 but also electrode reaction kinetics, which was in fact observed in experimental measurements (vide infra).

Experimentally, Co^{2+}-doped $Li_{2-x}O_2$ was found to also exhibit remarkable stability (Figure S6), as manifested in proton nuclear magnetic resonance (^1H NMR) measurements where no apparent variation of the chemical shifts of the electrolyte was observed before and after electrochemical cycling (Figure S7 and S8).[57] Three SCLABs were then fabricated with the addition of different concentrations of $CoCl_2$ into the electrolyte, SCLAB-1 (0.5 M), SCLAB-2 (0.1 M), and SCLAB-3 (0.01 M), such that Co^{2+} could be doped in situ into the discharge product Li_2O_2. The experimental details are included in the Supporting Information. The SCLAB-2 battery displayed an onset potential of 2.30 V for reduction in Ar (Figure S9), which was lower than that in O_2 (2.74 V). This was attributed to the ORR in aprotic LAB, and the voltage window was restricted to 2.4 - 4.3 V to avoid possible side reactions in subsequent tests.

Figure 2a shows the scanning electron microscopy (SEM) images of the SCLAB-2 electrode after being discharged to 2.4 V. One can see that nanosheet arrays were produced on the electrode surface with a thickness of *ca*. 10 nm. This morphology is completely different from that in TLAB where toroidal Li_2O_2 was formed (Figure 2c). As suggested in DFT calculations (Figure 1), the doping of Co^{2+} into Li_2O_2 resulted in a distortion of the crystal lattice. Such a lattice strain could tune the energy of specific facets, where the higher growth rate on the transverse high planes than on the longitudinal low planes led to the formation of a low crystalline and even amorphous structure.[58-60] Additional contributions might arise from the strong adsorption of Li_2O_2 onto the Co-Li_2O_2 slab (Figure S4).[23, 61] This structural disparity most likely originated from the different electrical conductivity of the discharge product, in which Co^{2+} doping led to electron-rich sites that facilitated the adsorption of O_2 and LiO_2 species.[23, 61] Notably, after charging to 4.3 V (Figure 2b), the SCLAB-2 electrode surface became significantly smoother. By contrast, for the cobalt-free TLAB after being discharged to 4.5 V, particulate structures remained clearly visible on the electrode surface (Figure 2d). This suggests high reversibility of SCLAB, as compared to TLAB. From X-ray diffraction (XRD) measurements, the discharge product was found to be mostly amorphous in SCLAB-2 (Figure S10), likely due to the distortion effect of cobalt doping (Figure 1), whereas Li_2O_2 could be clearly identified in TLAB (Figure S11), which was decomposed in the subsequent charge process.

X-ray photoelectron spectroscopy (XPS) measurements were then carried out to unravel the compositional variations. From the survey spectra in Figure 2e one can see that the O/C ratio and the intensity of Li in SCLAB-2 decreased dramatically when discharge was switched to charge, suggesting ready decomposition of $Li_{2-x}O_2$. Deconvolution of the corresponding O 1s spectra in

Figure 2f yields three peaks at 531.03, 531.92, and 533.40 eV for the discharged electrode, which can be assigned to C-O, Li/Co-O and C=O, respectively. After charge, these species remained visible in the spectra, due to the formation of a solid electrolyte interface and residual Co-O_x species on the electrode surface. Meanwhile, the binding energy of the Li 1s electrons (Figure 2g) was found to increase to 55.46 eV from 55.20 eV in TLAB (Figure S12), likely due to the doping of high-electronegativity Co^{2+}. After charge, the Li content decreased drastically, due to the ready decomposition of $Li_{2-x}O_2$, and the small Li-residuals suggest high reversibility of $Li_{2-x}O_2$ after Co^{2+} doping.

As for the Co^{2+} 2p spectra (Figure 2h), a trace amount was found in the discharge product with a Co/Li atomic ratio of ca. 1:48 (close to that of $CoLi_{62}O_{64}$ in the supercell used in DFT calculations, Figure 1) and consistent with the results from elemental mapping measurements (Figure S13). In fact, when discharged to 2.4 V the Co 2p signals were rather apparent, due to the production of a significant amount of discharge product Co^{2+}-$Li_{2-x}O_2$, and after charge to 3.9 V, about 2/3 of the discharge product was decomposed resulting in a drastic diminishment of the Co 2p signal. The small content of the Co-O species in the $Li_{2-x}O_2$ matrix served not only as dopants, but also as electrocatalytic active sites for the ORR and OER processes.[19, 20] After full charge, a small fraction of the Co species remained, due to reaction of Co^{2+} with the highly active O_2^{2-} in battery operation. The resulting Co-O species acted as the active sites in the next cycle and cooperated with the Co^{2+} ions in electrolyte to construct a high-performance battery system.

The reversibility of SCLAB-2 was further investigated by the limited capacity strategy to avoid deep polarization. After operation for an extended period of time (Figure S14-S15), there was little Co-O species deposited onto the electrode surface, suggesting that the main reaction was based on the self-catalytic reaction in low overpotential cycles. In the subsequent high overpotential cycles, Co^{2+} ions partly remained, likely in the form of Co-O_x that acted as the self-catalysis sites (vide infra).

The combination of the DFT results and experimental data demonstrates that the improved performance was most likely due to the following favorable factors. Firstly, Co^{2+} doping enhanced the conductivity of Li_2O_2, which boosted the reaction kinetics. Meanwhile, as molecular orbital principles[62] indicate that the e_g electrons of Co^{2+} can be readily transferred to O, Co^{2+} doping is anticipated to lead to favorable adsorption of oxygen and oxygen-rich LiO_2 species. Secondly, the resulting Co-Li_2O_2 clusters could serve as catalysts for effective adsorption of Li_2O_2 molecules (Figure S4), and retain the high conductivity after adsorption, a unique advantage of self-catalytic

product. Thirdly, Co^{2+} doping can affect the structure of the oxygen p electrons in Co-Li_2O_2 leading to enhanced activity (Figure S5).[55] Finally, the doped product exhibited a sheet-like, amorphous array structure, which was conducive to decomposition in the charge process,[23, 39] in sharp contrast to TLAB where Li^+ deintercalatation occurred first, followed by bulk oxidation. With the help of the self-catalytic sites, the reaction kinetics was further improved.

Figure S16 shows the operation curve of SCLAB-2 in an Ar atmosphere, where almost no discharge capacity can be observed above 2.4 V. This indicates that the capacity observed in the oxygen atmosphere was due to the ORR process of LAB, rather than side reactions of Co^{2+} itself at this potential, as manifested in CV measurements.

The introduction of additives also led to a reduced charge-transfer resistance (R_{ct}), as manifested in electrochemical impedance spectroscopy measurements (Figure S17-S18 and Table S2), and R_{ct} was the lowest with the addition of $CoCl_2$. **Figure 3**a compares the performances of SCLABs and TLAB. The specific capacities were found to be 34,013 mAh g^{-1} for SCLAB-1, 20,650 mAh g^{-1} for SCLAB-2, and 15,061 mAh g^{-1} for SCLAB-3, about 7, 4, and 3 times higher than that (5,024 mAh g^{-1}) of TLAB, respectively. Such a capacity is also higher than that of the Co/C electrode (7,200 mAh g^{-1}, Figure S19, S20 and S21a). Notably, one can see that the higher the concentration of the $CoCl_2$ additive, the higher capacity and lower charge potential. This provides compelling evidence that Co species indeed served as the active sites and improved the electrocatalytic performance. In fact, only a single SCLAB-3 battery was needed to light a LED (inset to Figure 3a), although it exhibited the lowest specific capacity among the three SCLABs. In addition, SCLAB-1 exhibited the lowest overpotential of 0.84 V at 200 mA g^{-1} in full discharge-charge profiles, a performance better than leading results in previous studies that involved, for instance, Co_3O_4/Ag electrocatalysts, Co/CoO-graphene self-supported cathode, $NiCo_2S_4$@NiO heterostructureed electrocatalysts, Co_3O_4-catalyzed LiOH chemistry, bifunctional PTIO redox mediators, Ru-N-C electrocatalysts, Nb_2C MXene electrocatalysts, mesoporous metallic pyrochlore, etc.[63-70]

One may notice that the charge capacity of SCLAB is higher than the discharge capacity. This may be attributed to the oxidation of Co^{2+} in the electrolyte during the charge process, as in the subsequent discharge, Co^{3+} was reduced to Co^{2+} and simultaneously some of the Co^{2+} was doped into the discharge product matrix. Figure 3b depicts the OER overpotential, battery overpotential and round-trip efficiency for the different battery systems. It can be seen that the three SCLABs all significantly outperformed TLAB, within the context of OER overpotential, battery overpotential

and ORR overpotential, SCLAB-1 (0.56, 0.84, 0.28 V) < SCLAB-2 (0.59, 0.90, 0.31 V) < SCLAB-3 (0.77, 1.09, 0.32 V) < TLAB (1.59, 1.91, 0.32 V). The round-trip efficiency of SCLABs was also higher than that of TLAB, SCLAB-1 (76.1%) > SCLAB-2 (74.6%) > SCLAB-3 (70.8%) > TLAB (58.0%).

The stability of the battery was then evaluated with the limited capacity strategy to avoid deep polarization. From the discharge-charge profiles in Figure 3c-3g, it can be seen that (i) swift polarization occurred in SCLAB-3, leading to a sudden death; (ii) SCLAB-2 exhibited an improved performance with a slow growth of polarization after 60 cycles; and (iii) SCLAB-1 showed a stable profile for at least 90 circles with lesser polarization than that of SCLAB-2 at 60th cycle. In fact, SCLAB-1 displayed the longest cycle life (>118 circles at 1,000 mAh g^{-1}) along with a 100% coulombic efficiency (Figure 3h), which was superior to those of SCLAB-2 (*ca.* 80 cycles), SCLAB-3 (*ca.* 20 cycles), and Co/C electrode (30 cycles with serious polarization, Figure S21b-c).

Figure S21a displays the performance of a LAB with the addition of 0.2 M LiCl. As an additive, LiCl improved the performance of the battery by enhancing the electrical conductivity, where the Cl^-/Cl_x^- couple acted as electron carriers.[71] The conductive Cl^- anions could provide an additional path for electron transfer to the Li_2O_2 surface, mitigating the restricted-conductance issue caused by the insulating nature of Li_2O_2.[72] Cl^- could also improve the performance of the ORR and OER electrocatalysis. As shown in the Figure S22, the addition of neat LiCl improved the battery performance, but the effect was minor. However, electrode polarization became intensified, and the charging voltage increased rapidly to over 4.3 V after 20 cycles, which confirmed its minor role in the electrochemical performance.

The introduction of inactive element Al^{3+} also had a marked impact on the charging and discharging properties of LAB (Figure S22b). In the Al^{3+}-doped system, the median voltage of the first discharge was ca. 2.9 V and the median voltage of the charge was ca. 3.8 V, a drastic improvement as compared to that of TLAB. This may be related to the enhanced electrical conductivity of the discharge product Li_2O_2, as manifested in DFT study (Figure 1). Concurrently, the Al-Li_2O_2 clusters served as interfacial catalysts displaying a strong adsorption energy for Li_2O_2 molecules (Figure S4), leading to a low discharge-charge overpotential (Figure S23). These reasons may jointly lead to the high discharge voltage of Al-Li_2O_2 during the first discharge-charge process, suggesting that heteroatom doping may be an effective strategy to mitigate the issues associated with insulating Li_2O_2 that traditionally limits the device performance.

Nevertheless, Al^{3+} or AlO_x did not contribute to the electrocatalytic performance, because they were inactive towards ORR/OER. Actually, with Al^{3+} deposited continuously onto the electrode surface, due to the high oxygen affinity, the polarization of the electrode was enhanced which caused battery death. Table S3 lists the LAB performances with different metal cation additives, where SCLAB can be seen to outperform other advanced cationic additive catalyst systems reported recently in the literature. Taken together, these results demonstrate the unique advantage of SCLABs with electrochemical doping of Co^{2+} into the $Li_{2-x}O_2$ matrix.

The SCLABs also exhibited fast charge kinetics, which was likely improved by the self-catalysis feature, especially in OER, due to the breaking of the solid-solid interface in traditional solid electrocatalysts. Notably, SCLABs did show a superior battery charge performance, as compared to others in the series. The promising results were demonstrated in **Figure 4**. One can see that SCLAB-1 could operate with a low overpotential of 0.13, 0.27, 0.50, and 0.69 V in charge at the current density of 200, 500, 1,000, and 3,000 mA g^{-1}, after discharge at 200 mA g^{-1} (discharge capacity limited to 500 mAh g^{-1}) (Figure 4a and 4b). This is significantly lower than the oxidation potential of Co^{2+}/Co^{3+} (> 3.8 V), indicating that the charge reaction was due to OER. By contrast, TLAB showed only a low round-trip efficiency in low rate (e.g., 500 mA g^{-1}) and almost no recharging (< 4.3 V) at high rates up to 3,000 mA g^{-1}. As well known, a lower charge potential indicates a lower energy barrier of the discharge decomposition, leading to improved kinetics. This may be ascribed to the enlarged O-O bond length (Figure 1).

Indeed, SCLAB-1 shows better reversibility and cyclability than TLAB (Figure 4c, S24 and S25). Even at high rates, e.g., 1,500 and 3,000 mA g^{-1} (20 and 10 min to recharge), the battery could operate 260 cycles (3,000 mA g^{-1}) without an apparent capacity decay, and the charge potential increased less than 6.43% (from 10^{th} to 180^{th} cycle). These results further confirm the significance of SCLABs in achieving high round-trip efficiency, fast charge/discharge kinetics and long cycle life.

The results presented above represent an effective approach to the optimization of LAB performance. For TLABs, battery death can occur due to the depletion of the metal anode. In addition, cathode failure is generally observed, where the air electrode is covered with undecomposable byproducts, such as Li_2CO_3 and organic lithium salts, and becomes inactive.[10, 12, 72] However, in SCLAB-1, after a long cycle operation, the morphology of the air electrode did not change significantly (**Figure 5**a and 5b). More importantly, there was almost no residual of Li-

containing compounds on the electrode surface, as evidenced in XPS measurements (Figure 5c). This implies that the cathode was not the key factor in compromising the battery life in SCLAB.

On the contrary, the structure of the SCLAB-1 anode changed greatly after cycling (Figure 5d-5g). After 10 cycles and death of the battery, the anode surface showed the formation of granulated structures (Figure 5g). Line-scan elemental analysis (Figure S26) shows that the anode was mainly composed of oxygen-containing compounds with almost no cobalt or chlorine. In previous studies, it has been argued that Li foil could be seriously powdered due to oxygen erosion.[73-75] Importantly, after replacing the Li foil and reassembling the battery (Figure 5h and 5i), the battery could again run stably, with a charging potential close to the previous one, as demonstrated in Figure 3f and 3g. That is, the sudden death of SCLABs was mainly due to the failure of the Li foil, rather than the cathode failure.

By combining DFT calculations and experimental results obtained above, we propose a mechanism for the enhanced performance of SCLABs (Figure 5j). Specifically, in the ORR process, Li^+ ions were transferred to the cathode forming Co^{2+}-doped $Li_{2-x}O_2$. This led to the formation of Co-O_x moieties that are electrocatalytically active towards oxygen electrocatalysis, and production of highly conductive $CoLi_{62}O_{64}$ clusters on the cathode surface as the main discharge product. In comparison to pristine Li_2O_2, $CoLi_{62}O_{64}$ exhibited a marked structural compression, with apparent variations of the Li-O and O-O bond lengths and Li-O-Li bond angle (Figure 1). This led to electron enrichment at the Co-O_x sites, and hence a reduced energy barrier for the decomposition of the discharge product.

3. Conclusion

In summary, in this study we demonstrated an in situ electrochemical doping strategy to significantly improve the performance of LAB. When metal ions were in situ embedded into the discharge product Li_2O_2 by adding appropriate metal salts into the electrolyte, marked structural compression occurred, which effectively facilitated the decomposition of Li_2O_2. Among the series, Co^{2+} stood out as the most effective dopant, where the resulting Co-O_x moieties in the $Li_{2-x}O_2$ matrix also served as the catalytic active sites for oxygen electrocatalysis. Electrochemically, the SCLAB system exhibited a markedly lowered overpotential of only 0.84 V in deep discharge-charge process and extended battery life of more than 118 cycles, as compared to TLAB. In addition, SCLAB could operate steadily in a high charge rate of 3,000 mA g^{-1} with 260 cycles, and fast charge to full capacity within 10 min. In combination with DFT studies, the remarkable performance of the SCLAB was largely ascribed to the enhanced electrical conductivity and

reduced energy barrier for the decomposition of the discharge product in the charge process. Results from this study highlight the significance of in situ structural engineering in enhancing the performance of electrochemical energy technologies.

Supporting Information

Supporting Information is available from the Wiley Online Library or from the author.

Acknowledgements

This project was supported by the National Natural Science Foundations of China (21771024, and 21871028) and China Postdoctoral Science Foundation (2020M680430).

Conflict of interest

The authors declare no competing financial interest.

Author Contributions

Dr. M. W. Yuan and Z. M. Sun contributed equally to this work. All authors discussed the results and contributed to writing the article.

Received: (will be filled in by the editorial staff)
Revised: (will be filled in by the editorial staff)
Published online: (will be filled in by the editorial staff)

References

[1] Z. Ma, X. Yuan, L. Li, Z. Ma, D. P. Wilkinson, L. Zhang, J. Zhang, *Energy Environ. Sci.* **2015,** *8*, 2144-2198.

[2] J. Shi, D. Xiao, X. Zhang, Y. Yin, Y. Guo, L. Gu, L. Wan, *Nano Res., Nano Res.* **2017,** *10*, 4201-4209.

[3] Y. Sun, T. Sun, X. Lin, X. Tao, D. Zhang, C. Zeng, A. Cao, L. Wan, *Sci. China Chem.* **2018,** *61*, 670-676.

[4] Z. Sun, X. Wu, Z. Gu, P. Han, B. Zhao, D. Qu, L. Gao, Z. Liu, D. Han, L. Niu, *Carbon* **2020,** *166*, 175-182.

[5] X. Wang, S. Wang, J. Qin, X. Xie, R. Yang, M. Cao, *Inorg. Chem.* **2019,** *58*, 16524-16536.

[6] W. Kwak, Rosy, D. Sharon, C. Xia, H. Kim, L. R. Johnson, P. G. Bruce, L. F. Nazar, Y. Sun, A. A. Frimer, M. Noked, S. A. Freunberger, D. Aurbach, *Chem. Rev.* **2020,** *120*, 6626-6683.

[7] B. Liu, Y. Sun, L. Liu, S. Xu, X. Yan, *Adv. Funct. Mater.* **2018,** *28*, 1704973.

[8] F. Li, Y. Chen, D.-M. Tang, Z. Jian, C. Liu, D. Golberg, A. Yamada, H. Zhou, *Energy Environ. Sci.* **2014,** *7*, 1648-1652.

[9] R. Black, J. H. Lee, B. Adams, C. A. Mims, L. F. Nazar, *Angew. Chem. Int. Ed.* **2013,** *52*, 392-396.

[10] Z. Peng, S. A. Freunberger, Y. Chen, P. G. Bruce, *Science* **2012,** *337*, 563-566.

[11] Y. S. Jeong, J. B. Park, H. G. Jung, J. Kim, X. Luo, J. Lu, L. Curtiss, K. Amine, Y. K. Sun, B. Scrosati, Y. J. Lee, *Nano Lett.* **2015,** *15*, 4261-4268.

[12] Z. Jian, P. Liu, F. Li, P. He, X. Guo, M. Chen, H. Zhou, *Angew. Chem. Int. Ed.* **2014,** *53*, 442-446.

[13] W. B. Luo, X. W. Gao, S. L. Chou, J. Z. Wang, H. K. Liu, *Adv. Mater.* **2015,** *27*, 6862-6869.

[14] J. Lu, Y. Lei, K. C. Lau, X. Luo, P. Du, J. Wen, R. S. Assary, U. Das, D. J. Miller, J. W. Elam, H. M. Albishri, D. A. El-Hady, Y. K. Sun, L. A. Curtiss, K. Amine, *Nat. Commun.* **2013,** *4*, 2383.

[15] J. Lu, Y. J. Lee, X. Luo, K. C. Lau, M. Asadi, H. H. Wang, S. Brombosz, J. Wen, D. Zhai, Z. Chen, D. J. Miller, Y. S. Jeong, J. B. Park, Z. Z. Fang, B. Kumar, A. Salehi-Khojin, Y. K. Sun, L. A. Curtiss, K. Amine, *Nature* **2016,** *529*, 377-382.

[16] T. Ogasawara, A. Debart, M. Holzapfel, P. Novak, P. G. Bruce, *J Am Chem Soc* **2006,** *128*, 1390-1393.

[17] X. Hu, F. Cheng, X. Han, T. Zhang, J. Chen, *Small* **2015,** *11*, 809-813.

[18] R. Gao, Z. Shang, L. Zheng, J. Wang, L. Sun, Z. Hu, X. Liu, *Inorg. Chem.* **2019,** *58* (8), 4989-4996.

[19] Y. Zhang, M. Hu, M. Yuan, G. Sun, Y. Li, K. Zhou, C. Chen, C. Nan, Y. Li, *Nano Res.* **2018,** *12*, 299-302.

[20] R. Gao, Z. Li, X. Zhang, J. Zhang, Z. Hu, X. Liu, *ACS Catal.* **2016,** *6*, 400-406.

[21] K. R. Yoon, K. Shin, J. Park, S. H. Cho, C. Kim, J. W. Jung, J. Y. Cheong, H. R. Byon, H. M. Lee, I. D. Kim, *ACS Nano* **2018,** *12*, 128-139.

[22] M. Asadi, B. Sayahpour, P. Abbasi, A. T. Ngo, K. Karis, J. R. Jokisaari, C. Liu, B. Narayanan, M. Gerard, P. Yasaei, X. Hu, A. Mukherjee, K. C. Lau, R. S. Assary, F. Khalili-Araghi, R. F. Klie, L. A. Curtiss, A. Salehi-Khojin, *Nature* **2018,** *555*, 502-506.

[23] Z. Sun, J. He, M. Yuan, L. Lin, Z. Zhang, Z. Kang, Q. Liao, H. Li, G. Sun, X. Yang, R. Long, Y. Zhang, *Nano Energy* **2019**, *65*, 103996.

[24] J. G. Kim, Y. Kim, Y. Noh, W. B. Kim, *ChemSusChem* **2015,** *8*, 1752-1760.

[25] D. Kundu, R. Black, B. Adams, K. Harrison, K. Zavadil, L. F. Nazar, *J. Phys. Chem. Lett.* **2015,** *6*, 2252-2258.

[26] D. Wu, Z. Guo, X. Yin, Q. Pang, B. Tu, L. Zhang, Y. G. Wang, Q. Li, *Adv. Mater.* **2014,** *26*, 3258-3262.

[27] M. Yuan, R. Wang, W. Fu, L. Lin, Z. Sun, X. Long, S. Zhang, C. Nan, G. Sun, H. Li, S. Ma, *ACS Appl. Mater. Interfaces* **2019,** *11*, 11403-11413.

[28] T. Liu, M. Leskes, W. Yu, A. J. Moore, L. Zhou, P. M. Bayley, G. Kim, C. P. Grey, *Science* **2015,** *350*, 530-533.

[29] Y. Chen, S. A. Freunberger, Z. Peng, O. Fontaine, P. G. Bruce, *Nat. Chem.* **2013,** *5*, 489-494.

[30] Y. Chen, X. Gao, L. R. Johnson, P. G. Bruce, *Nat. Commun.* **2018,** *9*, 767.

[31] J. Zhang, B. Sun, Y. Zhao, A. Tkacheva, Z. Liu, K. Yan, X. Guo, A. M. McDonagh, D. Shanmukaraj, C. Wang, T. Rojo, M. Armand, Z. Peng, G. Wang, *Nat. Commun.* **2019,** *10*, 602.

[32] X. Gao, Y. Chen, L. Johnson, P. G. Bruce, *Nat. Mater.* **2016,** *15*, 918.

[33] Q. Zhao, N. Katyal, I. D. Seymour, G. Henkelman, T. Ma, *Angew. Chem. Int. Ed.* **2019,** *58*, 12553-12557.

[34] X. Shen, S. Zhang, Y. Wu, Y. Chen, *ChemSusChem* **2019**, *12*, 104-114.

[35] Q. Lin, Z. Cui, J. Sun, H. Huo, C. Chen, X. Guo, *ACS Appl. Mater. Interfaces* **2018,** *10*, 18754-18760.

[36] J. Fu, X. Guo, H. Huo, Y. Chen, T. Zhang, *ACS Appl. Mater. Interfaces* **2019,** *11*, 14803-14809.

[37] W. Dai, X. Cui, X. Chi, Y. Zhou, J. Yang, X. Lian, Q. Zhang, W. Dong, W. Chen, *ACS Appl. Mater. Interfaces* **2020,** *12*, 4558-4564.

[38] Z. Lyu, T. Wang, R. Guo, Y. Zhou, J. Chen, X. Wang, M. Lin, X. Tian, M. Lai, L. Peng, L. Wang, Z. Peng, W. Chen, *J. Mater. Chem. A* **2019,** *7*, 10389-10396.

[39] Y. Zhang, Q. Cui, X. Zhang, W. McKee, Y. Xu, S. Ling, H. Li, G. Zhong, Y. Yang, Z. Peng, *Angew. Chem. Int. Ed.* **2016,** *55*, 10717-10721.

[40] R. Gao, X. Liang, P. Yin, J. Wang, Y. L. Lee, Z. Hu, X. Liu, *Nano Energy* **2017,** *41*, 535-542.

[41] J. Lu, Y. J. Lee, X. Luo, K. C. Lau, M. Asadi, H. H. Wang, S. Brombosz, J. Wen, D. Zhai, Z. Chen, D. J. Miller, Y. S. Jeong, J. B. Park, Z. Z. Fang, B. Kumar, A. Salehi-Khojin, Y. K. Sun, L. A. Curtiss, K. *Nature* **2016,** *529*, 377-382.

[42] R. Asahi, T. Morikawa, T. Ohwaki, K. Aoki, Y. Taga, *Science* **2001,** *293*, 269-271.

[43] K. Gong, F. Du, Z. Xia, M. Durstock, L. Dai, *Science* **2009,** *323*, 760-764.

[44] Z. Kang, H. Guo, J. Wu, X. Sun, Z. Zhang, Q. Liao, S. Zhang, H. Si, P. Wu, L. Wang, Y. Zhang, *Adv. Funct. Mater.* **2019,** *29*, 1807031.

[45] X. Wang, Y. Zhang, H. Si, Q. Zhang, J. Wu, L. Gao, X. Wei, Y. Sun, Q. Liao, Z. Zhang, K. Ammarah, L. Gu, Z. Kang, Y. Zhang, *J. Am. Chem. Soc.* **2020,** *142*, 4298-4308.

[46] B. Wang, Y. Cheng, H. Su, M. Cheng, Y. Li, H. Geng, Z. Dai, *ChemSusChem* **2020**, *13* 4078-4085.

[47] M.Y. Wang, J.Z. Guo, Z.W. Wang, Z.Y. Gu, X.J. Nie, X. Yang, X.L. Wu, *Small* **2020**, *16*, 1907645.

[48] Z.Y. Gu, J.Z. Guo, X.X. Zhao, X.T. Wang, D. Xie, Z.H. Sun, C.D. Zhao, H.J. Liang, W.H. Li, X.L. Wu, *InfoMat* **2021**, *3*, 694-704.

[49] S.-F. Li, Z.-Y. Gu, J.-Z. Guo, X.-K. Hou, X. Yang, B. Zhao, X.-L. Wu, *J. Mater. Sci. Technol.* **2021**, *78*, 176-182.

[50] W. Dai, X. Cui, X. Chi, Y. Zhou, J. Yang, X. Lian, Q. Zhang, W. Dong, W. Chen, *ACS Appl. Mater. Interfaces* **2020,** *12*, 4558-4564.

[51] Y. J. Jun, S. H. Park, S. I. Woo, *ACS Comb. Sci.* **2014,** *16*, 670-677.

[52] A. Wang, Z. Zou, D. Wang, Y. Liu, Y. Li, J. Wu, M. Avdeev, S. Shi, *Energy Storage Mater.* **2020,** *35*, 595-601.

[53] H. Yu, K. N. Dinh, Y. Sun, H. Fan, Y. Wang, Y. Jing, S. Li, M. Srinivasan, Q. Yan, *Nanoscale* **2018,** *10*, 14877-14884.

[54] Z. M. Sun, L. Lin, Y. Q. Wei, M. W. Yuan, H. F. Li, C. Y. Nan, K. B. Yin, G. B. Sun, R. Long, X. J. Yang, *J. Mater. Chem. A* **2019,** *7*, 21918-21926.

[55] Y. Gong, W. Ding, Z. Li, R. Su, X. Zhang, J. Wang, J. Zhou, Z. Wang, Y. Gao, S. Li, P. Guan, Z. Wei, C. Sun, *ACS Catal.* **2018,** *8*, 4082-4090.

[56] M. W. Yuan, S. T. Zhang, L. Lin, Z. M. Sun, H. Yang, H. F. Li, G. B. Sun, C. Y. Nan, S. L. Ma, *ACS Sustainable Chem. Eng.* **2019,** *7*, 17464-17473.

[57] J. J. Xu, Z. W. Chang, Y. B. Yin, X. B. Zhang, *ACS Cent. Sci.* **2017,** *3*, 598-604.

[58] Q. Yuan, P. Li, J. Liu, Y. Lin, Y. Cai, Y. Ye, C. Liang, *Chem. Mater.* **2017**, *29*, 10198-10205.

[59] J. Yang, Z. Zeng, J. Kang, S. Betzler, C. Czarnik, X. Zhang, C. Ophus, C. Yu, K. Bustillo, M. Pan, J. Qiu, L.-W. Wang, H. Zheng, *Nat. Mater.* **2019**, *18*, 970-976.

[60] H. Yang, M. Yuan, Z. Sun, D. Wang, L. Lin, H. Li, G. Sun, *ACS Sustainable Chem. Eng.* 2020, 8, 8348-8355.

[61] J. Xiao, D. Mei, X. Li, W. Xu, D. Wang, G.L. Graff, W.D. Bennett, Z. Nie, L.V. Saraf, I.A. Aksay, J. Liu, J.-G. Zhang, *Nano Lett*. **2011**, *11*, 5071-5078.

[62] J. Suntivich, K.J. May, H.A. Gasteiger, J.B. Goodenough, Y. Shao-Horn, *Science* **2011**, *334*, 1383-1385.

[63] R. Gao, Z. Yang, L. Zheng, L. Gu, L. Liu, Y. Lee, Z. Hu, X. Liu, *ACS Catal.* **2018,** *8*, 1955-1963.

[64] P. Zhang, R. Wang, M. He, J. Lang, S. Xu, X. Yan, *Adv. Funct. Mater.* **2016,** *26*, 1354-1364.

[65] P. Wang, C. Li, S. Dong, X. Ge, P. Zhang, X. Miao, R. Wang, Z. Zhang, L. Yin, *Adv. Energy Mater.* **2019,** *9*, 1900788.

[66] J. Lu, S. Dey, I. Temprano, Y. Jin, C. Xu, Y. Shao, C. P. Grey, *ACS Energy Lett.* **2020,** *5*, 3681-3691.

[67] C. Xu, G. Xu, Y. Zhang, S. Fang, P. Nie, L. Wu, X. Zhang, *ACS Energy Lett.* **2017,** *2*, 2659-2666.

[68] X. Hu, G. Luo, Q. Zhao, D. Wu, T. Yang, J. Wen, R. Wang, C. Xu, N. Hu, *J. Am. Chem. Soc.* **2020,** *142*, 16776-16786.

[69] G. Li, N. Li, S. Peng, B. He, J. Wang, Y. Du, W. Zhang, K. Han, F. Dang, *Adv. Energy Mater.* **2020,** *11*, 2002721.

[70] S. H. Oh, R. Black, E. Pomerantseva, J.-H. Lee, L. F. Nazar, *Nat. Chem.* **2012,** *4*, 1004-1010.

[71] J. Zhang, B. Sun, Y. Zhao, K. Kretschmer, G. Wang, *Angew. Chem. Int. Ed.* **2017,** *56*, 8505-8509.

[72] S. A. Freunberger, Y. Chen, N. E. Drewett, L. J. Hardwick, F. Barde, P. G. Bruce, *Angew. Chem. Int. Ed.* **2011,** *50*, 8609-8613.

[73] K. R. Adair, C. Zhao, M. N. Banis, Y. Zhao, R. Li, M. Cai, X. Sun, *Angew. Chem. Int. Ed.* **2019,** *58*, 15797-15802.

[74] Z. Huang, H. Zeng, M. Xie, X. Lin, Z. Huang, Y. Shen, Y. Huang, *Angew. Chem. Int. Ed.* **2019,** *58*, 2345-2349.

[75] Q. C. Liu, J. J. Xu, S. Yuan, Z. W. Chang, D. Xu, Y. B. Yin, L. Li, H. X. Zhong, Y. S. Jiang, J. M. Yan, X. B. Zhang, *Adv. Mater.* **2015,** *27*, 5241-5247.

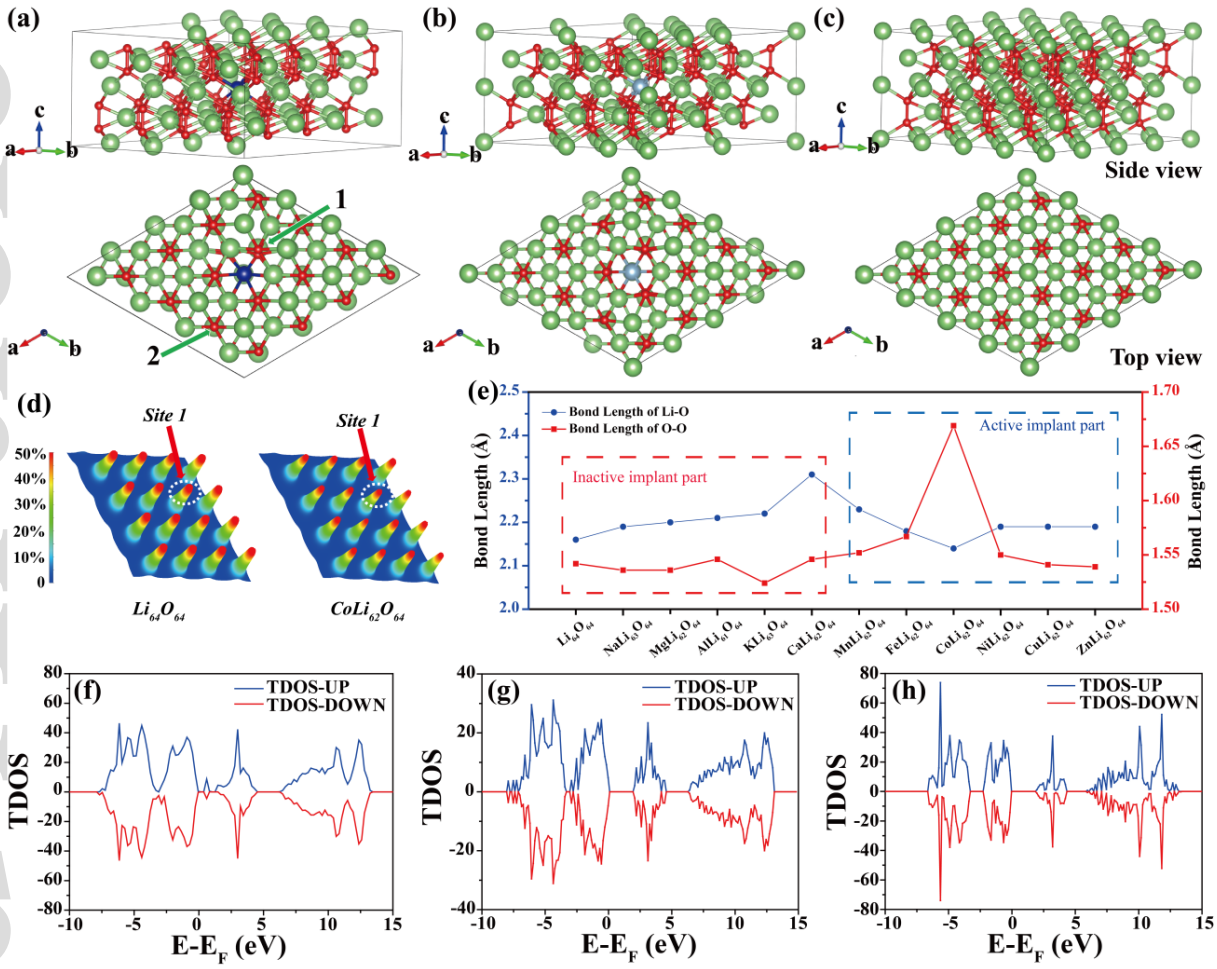

Figure 1. Optimized structures of (a) $CoLi_{62}O_{64}$, (b) $AlLi_{61}O_{64}$ and (c) $Li_{64}O_{64}$. (d) Charge distribution of O layer for $CoLi_{62}O_{64}$ and $Li_{64}O_{64}$. (e) Bond length of Li-O and O-O (site 1) with different elements implanting systems. TDOS of (f) $CoLi_{62}O_{64}$, (g) $AlLi_{61}O_{64}$ and (h) $Li_{64}O_{64}$ Optimized structure of $CoLi_{62}O_{64}$ and $AlLi_{61}O_{64}$ hided one Li atom on the top of Co and Al to show clear structure. Red, blue, grey and green balls represent the O, Co, Al and Li atoms, respectively.

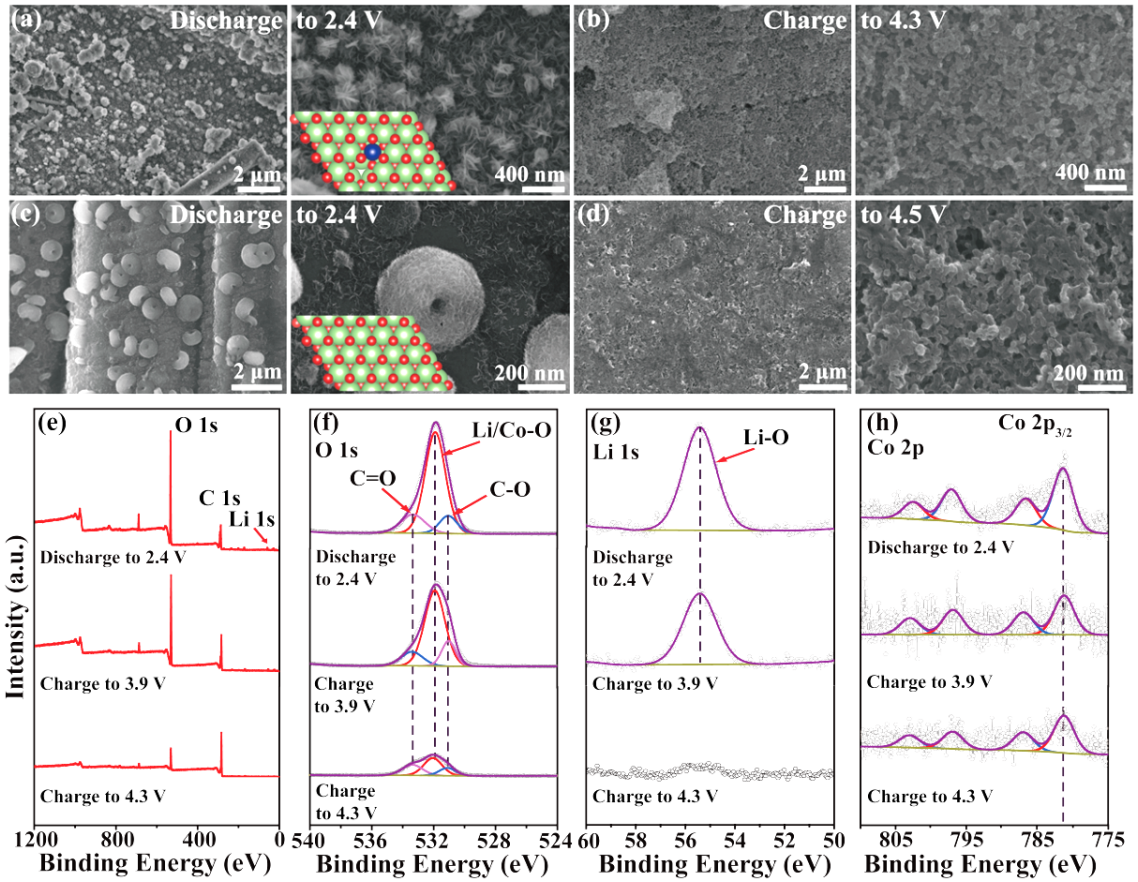

Figure 2. SEM images of discharged and charged electrode in (a, b) SCLAB-2 and (c, d) TLAB. Insets to panels (a) and (c) are the respective sample structures. (e) Survey spectra and (f-h) high-resolution scans of the (f) O 1s, (g) Li 1s and (h) Co 2p electrons of the SCLAB electrodes at different states.

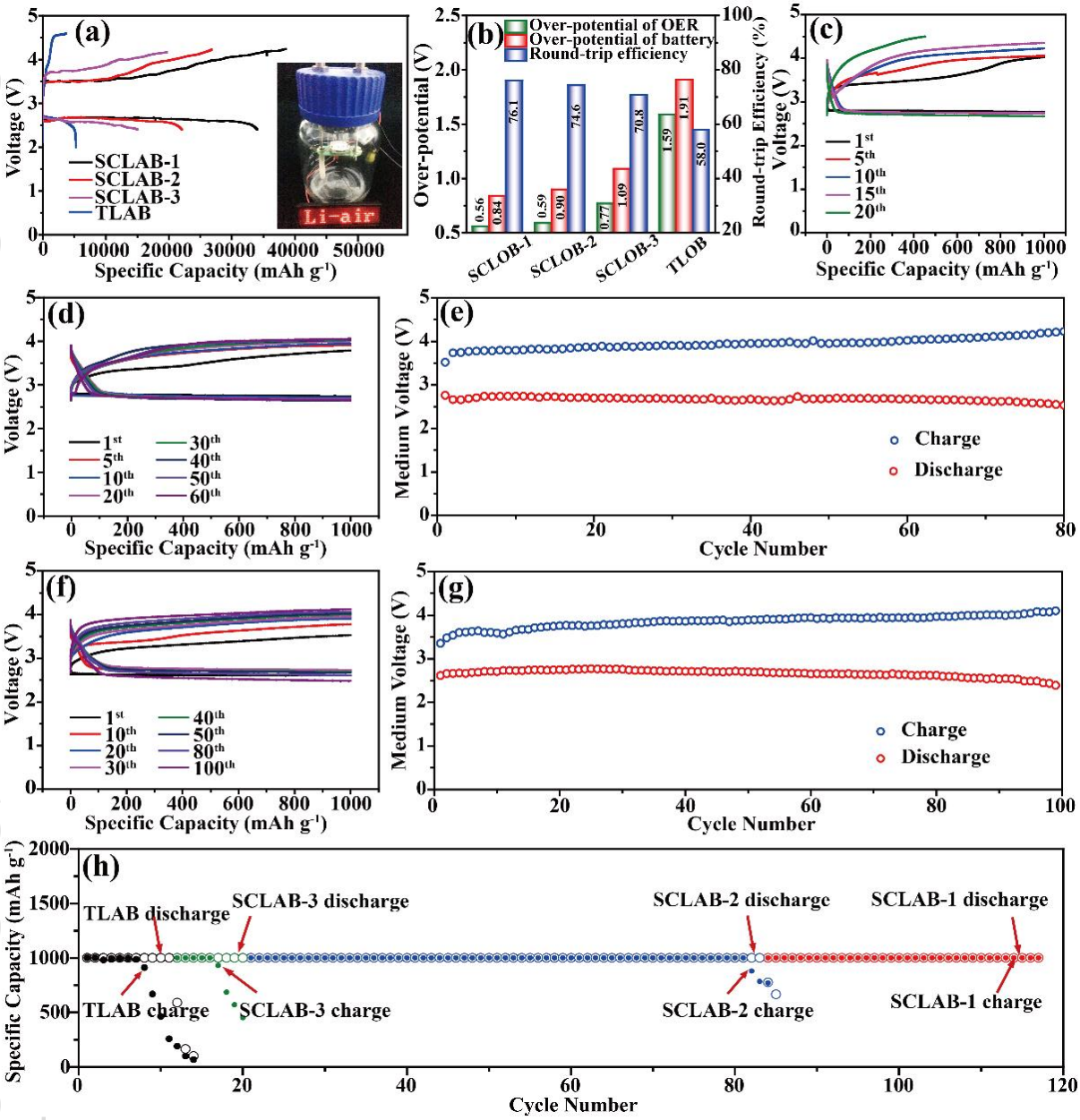

Figure 3. (a) Full discharge-charge profiles and (b) histogram of overpotential and round-trip efficiency in different battery systems. Inset to panel (a) is a photograph where a LED is lit by a single SCLAB-3. Discharge-charge profiles and voltage variation with a limited specific capacity for (c) SCLAB-3, (d, e) SCLAB-2, and (f, g) SCLAB-1. (h) Cyclability comparison of different battery systems at a specific capacity of 1000 mAh g^{-1}. All current density is fixed at 200 mA g^{-1}.

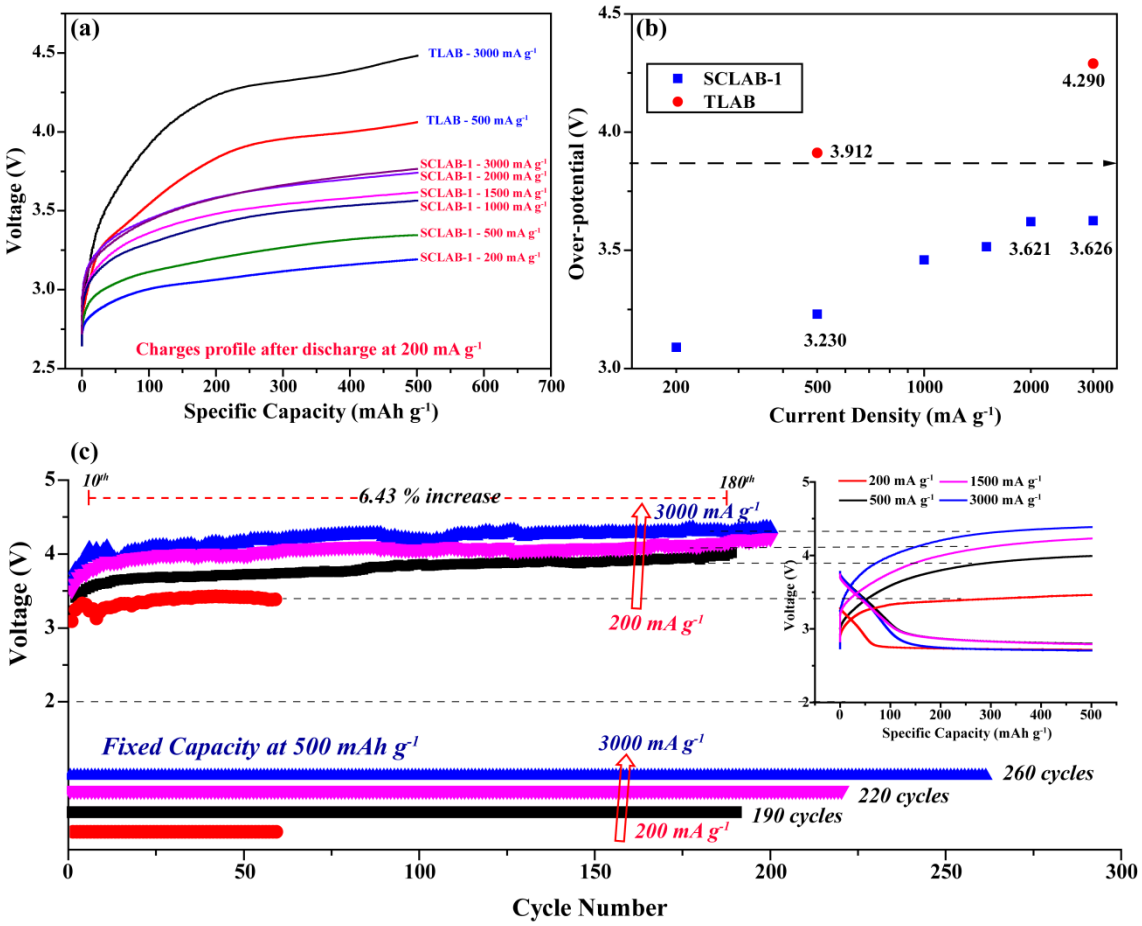

Figure 4. (a) Charge profiles and (b) medium voltage in charge of SCLAB-1 and TLAB at different charge rate. (c) Variation of capacity retention and medium voltage in charge for SCLAB at different charge rates. Inset to panel (c) is the discharge-charge profiles in various cycles (60th at 200 mA g^{-1}, 150th at 500 mA g^{-1}, 175th and 180th at 1500 and 3000 mA g^{-1}). All the batteries operated at the same discharge current density of 200 mA g^{-1}, and then charged at different current density to evaluate the fast charge properties.

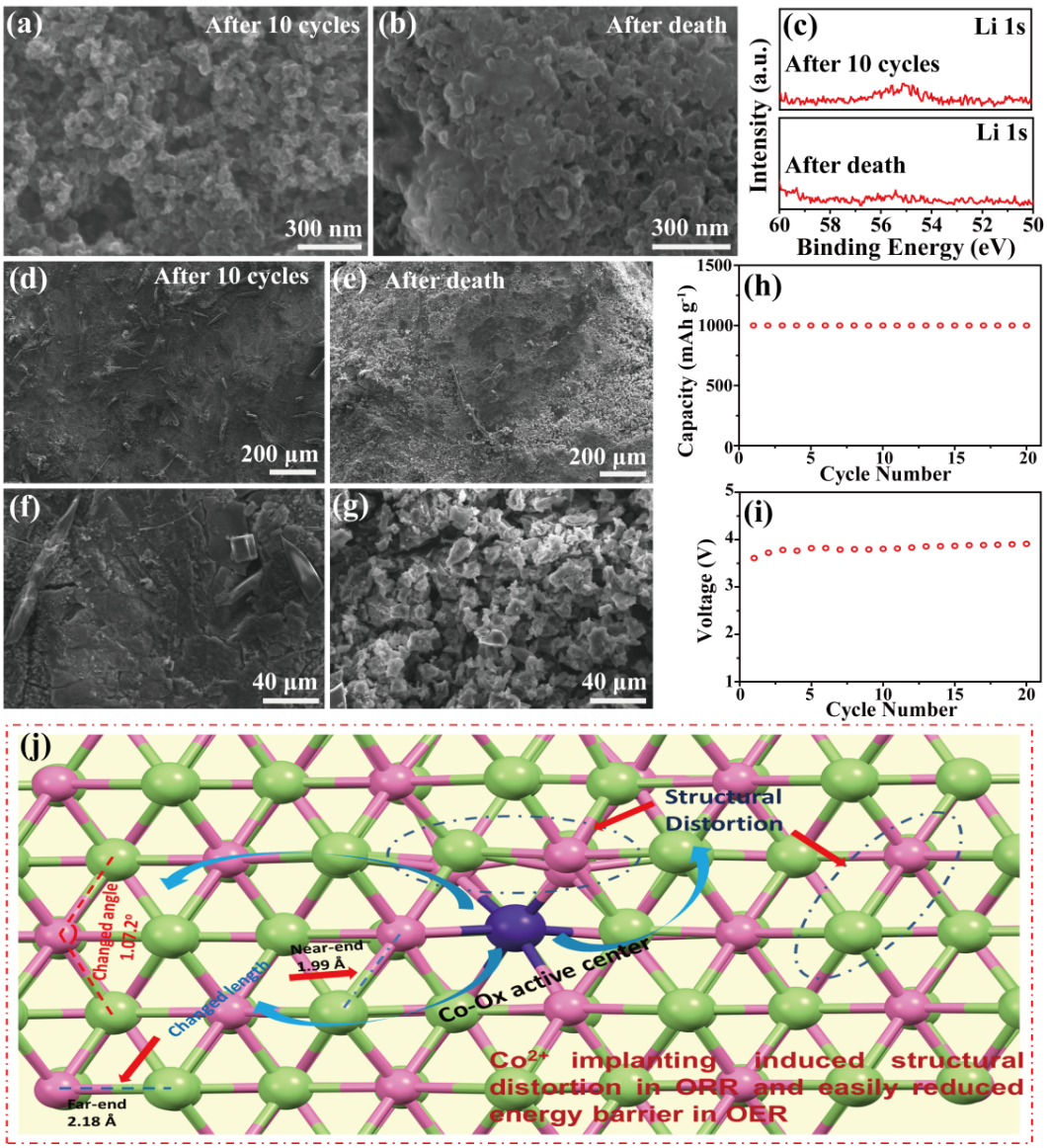

Figure 5. (a, b) SEM images and (c) XPS spectra of the Li 1s electrons of the SCLAB-1 cathode after 10 cycles and battery death. SEM images of the Li foil in SCLAB-1 after (d, e) 10 cycles and (f, g) battery death. (h) Cyclability and (i) charge voltage of the SCLAB-1 re-assembled with a new Li foil. (j) Schematic illustration of important reactions with Co^{2+} doping in SCLAB.

Table of content

In-situ doping of Li_2O_2 by Co^{2+} is found to significantly enhance the performance of lithium-air battery, as manifested in theoretical and experimental studies. This is ascribed to the unique catalytic activity of the resulting Co-O_x sites towards oxygen electrocatalysis and the structural compression upon Co^{2+} doping that boosts electrode reaction kinetics.